韓國航海港灣學會 第26卷 第2號 pp. 127~132

論 文

Space and Time Sensor Fusion Using an Active Camera For Mobile Robot Navigation

Tae-Seok Jin, Bong-Ki Lee*, Soo-Min Park*, Kwon-Soon Lee**, and Jang-Myung Lee***

*Dept. of Electronics Engineering, Pusan Nat'l Univ., Pusan, 609-735, korea
**Dept. of Electrical Engineering, Dong-A Univ., Pusan, 604-714, korea

Abstract **-- This paper proposes a sensor-fusion technique where the data sets for the previous moments are properly transformed and fused into the current data sets to enable accurate measurement, such as, distance to an obstacle and location of the service robot itself. In the conventional fusion schemes, the measurement is dependent on the current data sets.**

As the results, more of sensors are required to measure a certain physical parameter or to improve the accuracy of the measurement. However, in this approach, instead of adding more sensors to the system, the temporal sequence of the data sets are stored and utilized for the measurement improvement. Theoretical basis is illustrated by examples and the effectiveness is proved through the simulations. Finally, the new space and time sensor fusion (STSF) scheme is applied to the control of a mobile robot in an unstructured environment as well as structured environment.

I. INTRODUCTION

So far many of researches have been done on the spatial fusion technique. That is, multiple sensor data are utilized either for the purpose of providing complementary or redundant data to measuring physical parameters. That is, all of the current data from the sensors are integrated and fused to obtain a correct set of data.

In recent years interest has been growing in the synergistic use of multiple sensors to increase the capabilities of intelligent machines and systems. For these systems to use multiple sensors effectively, some method is needed for integrating the information provided by these sensors into the operations of the system.

In this new approach, the data obtained by the sensors are utilized until they do not have any efficiency for the measurement decision. The data set can be either redundant to improve the accuracy or complementary for the measurement. For the later case, this space and time sensor fusion is essential for the measurement.

The space and time fusion is inevitable for the complementary case. Therefore the effectiveness is very clear and the utilization method will be determined by the sensory data structure. However for the redundant case, it is required to define that how to fuse the previous data sets to the current data set. In this paper, we are basically going to utilize the minimum square solution for the fusion scheme without considering the error variance in the measurement for simplicity.

II. SPACE AND TIME SENSOR FUSION

Multi-sensor fusion refers to any stage in the integration process where there is an actual combination (or fusion) of different sources of sensory information into one representational format.

2.1. A General Pattern of Sensor Fusion

Figure 1 means to represent a general pattern of multi-sensor integration and fusion in a system. In this figure, *n* sensors are integrated to provide information to the system.

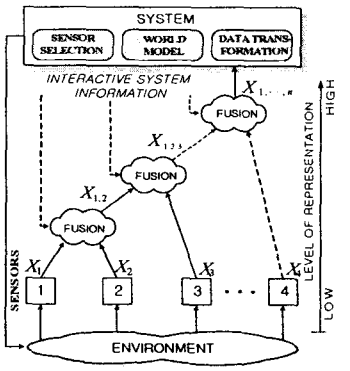

Fig. 1 General pattern of multi-sensor integration and fusion in system.

The output x_1 and x_2 from the first two sensors are fused at the lower left-hand node into a new representation $x_{1,2}$. The output x_3 from the third sensor could then be fused with $x_{1,2}$ at the next node, resulting in the representation $x_{1,2,3}$, which might then be fused at nodes higher in the structure.

2.2. Sensor Fusion Transformation

Let us define the *k*-th moment data set provided by *i*-th sensor as, $\mathbf{z_i(k)}$, and the *k*-th measurement vector as $\mathbf{x(k)}$. Then the conventional sensor fusion technique provides the measurement as

$$\hat{x}(k) = \sum_{i=1}^{n} W_i x_i(k) \qquad (1)$$

where $x_i(k) = H_i z_i(k) \in R^m$,

H_i represents transformation from the sensory data to the measurement vector, and $W_i \in R^{m \times m}$ represents the weighting value for *i*-th sensor.

Note that in the measurement of $\mathbf{z_i(k)}$, the low-level fusion might be applied with multiple sets of data with known statistics[2]. The determination of H_i is purely dependent on the sensory information and the decision of W_i can be done through the sensor fusion process. Later this measured data are provided to the linear model of the control/measurement system as current state vector, $\mathbf{x(k)}$. In this approach, we propose a multi-sensor data fusion using sensory data, $Tz_i(j)$,

as

$$\hat{x}(k) = \sum_{i=1}^{n} W_i \{ \sum_{j=1}^{k} P_j Tz_i(j) \} \quad (2)$$

where $\sum_{j=1}^{k} P_j = 1$.

Note that when each of sensor information can provide the measurement vector, that is, the redundant case, $Tz_i(j)$ can be expanded as

$$Tz_i(j) = T_j + H_i z_i(j) \quad (3)$$

where T_j represents the homogeneous transformation from the location of the j-th to the k-th measurements.

However, when the multi-sensors are utilized in the complementary mode, the transformation relationship cannot be defined uniquely; instead it will be defined depending on the data constructing algorithm from the measurements. For example, a single image frame captured by a camera on a mobile robot cannot provide the distance to an object until the corresponding object image is provided again from a different location. This algorithm will be described in detail in the section 3.1.

Figure 2 illustrates the concept of this multi-sensor temporal data fusion. Estimation of parameter may provide the measurement vector at each sampling moment. The verification of significance and adjustment of weight steps are pre-processing stages for the sensor fusion. After these steps, the previous data set will be fused with the current data set, which provides a reliable and accurate data set as the result of multi-sensor temporal fusion. Significance implies that how much the previous data set is related to the current data. An arbitrary value of significance may cause the problem to be complex. Therefore, here we may consider whether it corresponds to the same data or not, that is, 1 or 0. When the significance is 0, the weight can be adjusted simply to be 0. However, when the significance equals 1, the adjustment of weight should be properly performed to provide reliable and accurate data. Here in the following sub-section, we introduce a simple methodology for the weight adjustment.

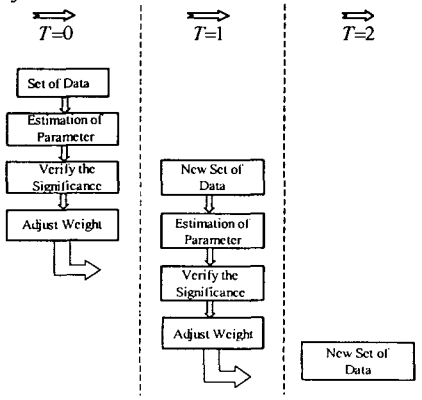

Fig. 2 Concept of Space and Time Sensor Fusion.

2.3. Auto-correlation for Estimation Techniques

Each previous data set is transformed to the k-th (current) sampling location, and represented by the measurement vector, $Tz_i(j)$. Now how can we fuse the k data sets into a reliable and accurate data set? In the Eq. (2), W_i can be determined by the geometrical relationship among sensors, in other words, by the spatial sensor fusion.

While the estimating sensor is tracking a feature, it generates a stream of measurements. When there is relative motion between the feature and the sensor, the processes then cease to be stationary. As an illustration of gathering the model information from the sensor, we shall only consider the stationary case, in order words, there is no motion between the sensor and the feature being tracked. Our interest in the proceeding analysis lies only in determining whether the process noise is white or not.

Random processes are defined in terms of their ensemble averages and these can be estimated. Our model shall be in terms of such averages. In practice, we require to estimate these averages from finite sequences. We consider a process y_k as realized (estimated) by the finite sequence $y(k)$, for $0 \le k \le N-1$. That $y(k)$ is an estimate of the random process y_k is made plausible by a consideration of ergodic processes. From $y(k)$, we can, therefore, estimate the averages for the process, the mean is estimated by $\hat{\mu}_x = \frac{1}{N}\sum_{k=0}^{N-1} x(k)$ and the variance by $\hat{\sigma}_x^2 = \frac{1}{N}\sum_{k=0}^{N-1}(x(k)-\mu_x)^2$,

A biased estimate of the autocorrelation is given by

$$\tilde{\phi}_{xx}(m) = \frac{1}{N}\sum_{k=0}^{N-|m|-1} x(k)\cdot x(k+m) \quad (4)$$

with a variance of $\tilde{\sigma}_{\tilde{x}} = \frac{1}{\sqrt{N}}\tilde{\sigma}_x^2$, (5)

where $|m| < N$. Similarly, an unbiased autocorrelation is estimated by

$$\hat{\phi}_{xx}(m) = \frac{1}{N-|m|}\sum_{k=0}^{N-|m|-1} x(k)\cdot x(k+m) \quad (6)$$

and the variance of the unbiased autocorrelation is given by

$$\hat{\sigma}_{\hat{\phi}} = \frac{\sqrt{N}}{N-|m|}\hat{\sigma}_x^2 \quad (7)$$

for the biased autocorrelation and similarly for the unbiased one. Therefore, determination of P_j is the final step for the temporal sensor fusion. Note that this expands the dimension of sensor fusion from one to two.

As one of solid candidate, we propose here to use the auto-correlation as an index for the weight adjustment and have the form,

$$\Psi_j = \sum_{k=-\infty}^{+\infty} x_i(k)x_i(j-k). \quad (8)$$

Depending on the correlation, P_j will be determined as

$$P_j = \frac{\Psi_j}{\sum_{j=1}^{k}\Psi_j} \quad (9)$$

III. Applications to Mobile Robots

3.1 Complementary Usage for 3D Vision

If the image for an object is well matched to one model in the database, the position of the object can be obtained directly. In a well-structured environment, it may be a usual case. However, when the mobile robot is navigating in an unstructured environment, it needs to recognize the position/orientation of an object located in the middle of its path, which is not known to the robot a priori.

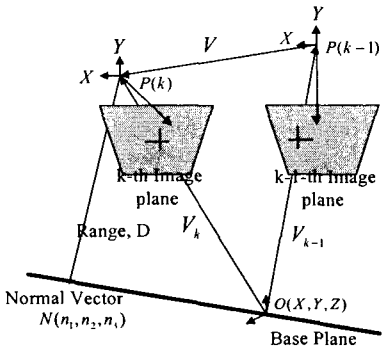

Fig. 3. Transformation of camera coordinates.

As a typical geometrical model for camera, a pinhole model is widely used in vision application fields as shown in Fig. 3. At the *k*-th sampling moment, a scene point O(X,Y,Z) is captured by a camera on the mobile robot. The vectors from the scene point to the *k*-th and *(k-1)*th camera perspective center are represented by V_k and V_{k-1}, respectively. The motion of mobile robot from *(k-1)*th moment to *k*-th moment is represented by *V*. Now we can write the vector relationship as

$$V_{k-1} = V_k - V \,. \tag{10}$$

This can be represented as a matrix form,

$$\alpha \begin{bmatrix} x_{k-1} \\ y_{k-1} \\ -f \end{bmatrix} = \beta \begin{bmatrix} r_{11} & r_{12} & r_{13} \\ r_{21} & r_{22} & r_{23} \\ r_{31} & r_{32} & r_{33} \end{bmatrix} \begin{bmatrix} x_k \\ y_k \\ -f \end{bmatrix} - \begin{bmatrix} v_1 \\ v_2 \\ v_3 \end{bmatrix} \tag{11}$$

where $(x_k, y_k, -f)$ and $(x_{k-1}, y_{k-1}, -f)$ represent the projection of the scene point onto the camera image planes; $V(v_1, v_2, v_3)$ represents the translational motion of the mobile robot; r_{ij} is an element of the rotation matrix, R represents the relative rotation between the two camera frames; α and β are constants.

Now consider the reference base plane passing through the scene point P with a direction vector $N(n_1, n_2, n_3)$; then the range value, *D*, can be represented as

$$D = V_k \cdot N \,. \tag{12}$$

This can be represented again as

$$D = \beta(n_1 x_k + n_2 y_k - n_3 f) \,. \tag{13}$$

Now, Eq. (11) is reformulated as

$$\alpha \begin{bmatrix} x_{k-1} \\ y_{k-1} \\ -f \end{bmatrix} = \beta \begin{bmatrix} r_{11} & r_{12} & r_{13} \\ r_{21} & r_{22} & r_{23} \\ r_{31} & r_{32} & r_{33} \end{bmatrix} \begin{bmatrix} x_k \\ y_k \\ -f \end{bmatrix} - \frac{\beta}{D} \begin{bmatrix} v_1 \\ v_2 \\ v_3 \end{bmatrix} \begin{bmatrix} n_1 & n_2 & n_3 \end{bmatrix} \begin{bmatrix} x_k \\ y_k \\ -f \end{bmatrix} \tag{14}$$

$$(\alpha/\beta) \begin{bmatrix} x_{k-1} \\ y_{k-1} \\ -f \end{bmatrix} = \begin{bmatrix} a_{11} & a_{12} & a_{13} \\ a_{21} & a_{22} & a_{23} \\ a_{31} & a_{32} & a_{33} \end{bmatrix} \begin{bmatrix} x_k \\ y_k \\ -f \end{bmatrix} \tag{15}$$

where $a_{ij} = r_{ij} - (v_i \cdot n_j / D)$.

Expanding the matrices and dividing rows one and two by row three gives

$$D(R_3 x_{k-1} + R_1 f) = C_3 x_{k-1} + C_1 f \tag{16}$$

$$D(R_3 y_{k-1} + R_2 f) = C_3 y_{k-1} + C_2 f \tag{17}$$

where $R_i = r_{i1} x_k + r_{i2} y_k - r_{i3} f$ and $C_i = v_i(n_1 x_k + n_2 y_k - n_3 f)$.

In matrix form, these equations can be expressed as

$$AD = B \tag{18}$$

where $A^T = [a \;\; b], B^T = [c \;\; d]$, $a = R_3 x_{k-1} + R_1 f$,

$b = R_3 y_{k-1} + R_2 f$, $c = C_3 x_{k-1} + C_1 f$, and $d = C_3 y_{k-1} + C_2 f$.

Use of the pseudo-inverse matrix enables computation of the range value, *D* which is associated with image point (x_k, y_k), and is written as,

$$D = (A^T A)^{-1} A^T B \text{ or} \tag{19}$$

$$D = \frac{(ac + bd)}{a^2 + b^2} \,. \tag{20}$$

So far, we have shown that using the consecutive two image frames, the distance information of the scene point can be obtained as using the stereo images at a certain moment.

3.2 Space and Time Fusion Filter

The space and time fusion consists of combining information acquired at different instants and then deciding the data. It implies that the system must be able to predict objects state at each instant (see Figure 4).

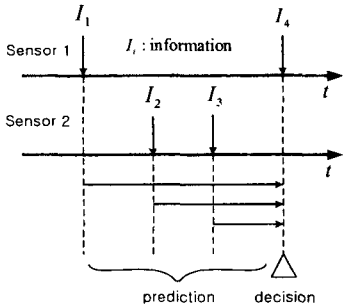

Fig. 4. An example of Space and Time fusion.

Given two estimators $\hat{\Theta}_1$ and $\hat{\Theta}_2$ of Θ, and the task is to fuse then together to form one single "optimal" estimate $\hat{\theta}$. Here, estimators are stochastic variables and are denoted by capital letters.

Assume that $\hat{\Theta}_1 - \Theta$ and $\hat{\Theta}_2 - \Theta$ are independent Gaussian distributed with zero mean and covariances P_1 and P_2, respectively. Now let $X = \Theta - \hat{\Theta}_1$ and $Y = \hat{\Theta}_2 - \hat{\Theta}_1$. Then $\Sigma_{xx} = P_1$ and $\Sigma_{yy} = P_1 + P_2$. Hence

$$\hat{x} = P_1(P_1 + P_2)^{-1}(\hat{x}_2 - \hat{x}_1) \tag{21}$$

$$\hat{\theta} = \hat{\theta}_1 + P_1(P_1 + P_2)^{-1}(\hat{\theta}_2 - \hat{\theta}_1) \text{ or} \tag{22}$$

$$\hat{\theta} = [P_1^{-1} + P_2^{-1}]^{-1}[P_1^{-1}\hat{\theta}_1 + P_2^{-1}\hat{\theta}_2], \tag{23}$$

with covariance

$$P_1 - P_1(P_1+P_2)^{-1}P_1 = [P_1^{-1}+P_2^{-1}]^{-1} . \quad (24)$$

The fusion formula just means that estimates should be weighted together, with weights inversely proportional to their qualities/variances. It is easy to modify the fusion filter to handle correlated estimators.

IV. Robot Type in Experiments Setup

The mobile robot used in the experiments is an *IRL-2001* developed in the *IRL*, PNU which is designed for an intelligent service robot.

This robot is shown in Figure 5 along with some of its sensory components. Its main controller is made on system clock 600 MHz, Pentium III Processor. The sensors, 16-ultrasonic and a robust odometry system are installed on the mobile robot. Ultrasonic sensors and infrared sensors in eight sides(25°) sense obstacles of close range, and the main controller processes this information.

For visual information, a CCD camera is mounted on the top of the mobile robot in order to sense obstacles or landmarks of the side and the rear of mobile robot. And DC servomotors are used for steering and driving of *IRL*-2001 robot.

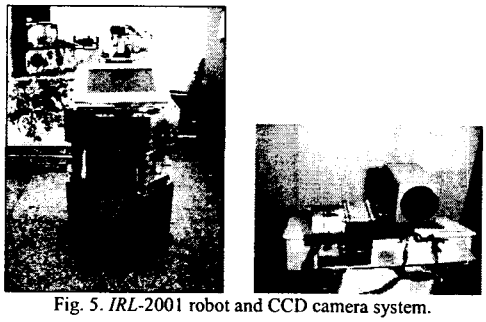

Fig. 5. *IRL*-2001 robot and CCD camera system.

V. Experimental Results

5.1 Robot Localization used Landmark pattern recognition

The service robot(*IRL*-2001) is commanded to follow the environment as shown from (a) to (f) of Figure 7. We performed the experiment for two cases.

To begin with, the 2-D landmark used by *IRL-2001* is shown in Figure 6. The primary pattern of landmark is a 10cm black square block on white background and a 5cm square block. The major reasons for choosing the square blocks are

- The projection of a square block in the image plane can always be approximated by an ellipse, which is easy to recognize using the elliptical Hough transformation technique.
- A square pattern is more robust to noise and occlusion than circular, polygonal patterns during template matching process, even though all these patterns can be detected by using Hough transformation technique.

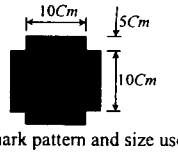

Fig. 6. The landmark pattern and size used by *IRL-2001*.

The image corners are then automatically extracted by camera parameters, and displayed on Figure 6 and the blue squares around the corner points show the limits of the corner finder window. The corners are extracted to an accuracy of about 0.1 pixel.

The extrinsic parameters, relative positions of the landmark with respect to the camera, are then shown in a form of a 3D plot as Figure 8. And on Figure 9, every camera position and orientation are represented by red pyramid, therefore we can see the location and the orientation of a mobile robot in the indoor environment.

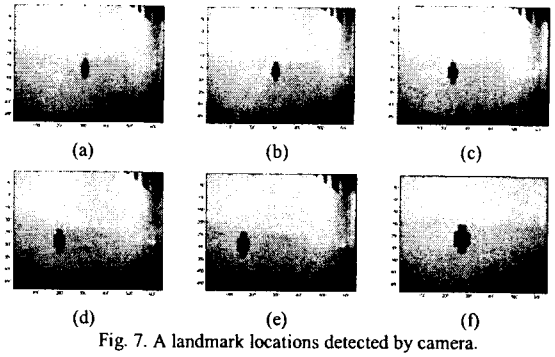

Fig. 7. A landmark locations detected by camera.

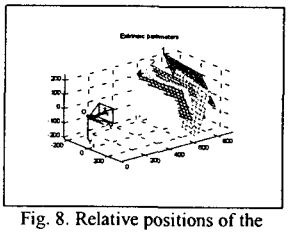

Fig. 8. Relative positions of the landmark w.r.t the camera.

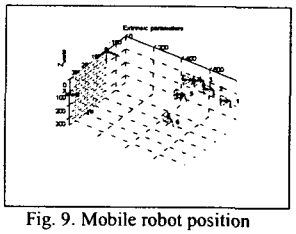

Fig. 9. Mobile robot position and orientation.

To measure the relative distance of the landmark from the mobile robot, we first measure the distance of image from the fixed position in *IRL*-lab corridor. The predefined values of the landmark defined in this section are given as follows the origin of coordinates is equal to the origin of mobile robot, a Y-axis is fit to the front of mobile robot and an X-axis is perpendicular with Y-axis.

Table 1 lists the data measured in *IRL*-lab corridor. The Left direction marks negative. From table 1, we find the maximum and the minimum error on distance is 0.32 m and 0.13m, respectively.

It shows that the distance error becomes less and less by frames, which composes the environment map. And so, we can use it to measure the relative distance of the mobile robot.

Table 1. The result of relative distance (Dim.:m).

Frame Number	World Coordinate Distance	Image Coordinate Distance	Error
1	7.81	8.13	0.32
2	7.02	7.30	0.28
3	6.28	6.53	0.25
4	5.06	4.89	0.17
5	5.52	5.39	0.13
6	6.32	6.46	0.14

5.2 Mobile robot Navigation

Conventional fusion and STSF(a space and time sensor fusion) have first been tested with simulation to show the usefulness of STSF in two environments respectively. Startin g at (0.3m, 5m, 0 degree), a virtual robot was driven around a virtual square corridor one time. The walls in the artificial en vironment are denoted by the real map, *IRL* corridor of PNU.

In each round, the robot stops a total of 12 times to rescan the environment. The size of given map is 12m X 8m, the total distance traveled is 12 + 8=20 meters, and the total num ber of scanning points is 38. The comparison of simulation p osition and direction at all stops is shown in Figure 10 and Figure 11.

Figure 10 shows determination of the pointing vector base d upon only current readings used conventional sensor fusio n, i.e. spatial fusion. This robot was made to move randomly within the confines of the above setup and at the region, *Cc*. There are a little of difference between conventional fusion and the new STSF. But at the region, *Ac*, the robot moves no t keeping the distance between robot and wall constant and have some difficult local minimum trap problems at some places.

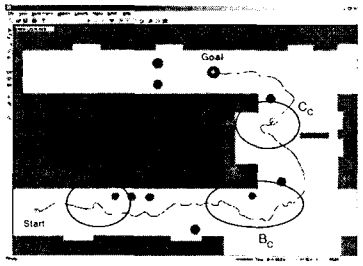

(a). Experiment in a corridor.

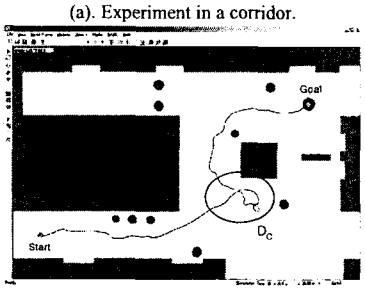

(b). Experiment in a corridor with wide space.

Fig. 10. Simulation for pointing vector based upon current readings.

Figure 11 shows multi-sensor STSF scheme is applied for the measurement. And the results are compared to show the superiority of the proposed scheme. The robot was allowed to move keeping the distance between robot and obstacles constant at the region, A_T and B_T.

The region B_T, shows the improvement in steering at cor ner. And the simulation experiments show that a mobile rob ot, utilizing our scheme, can avoid obstacles and reach a giv en goal position in the workspace of a wide range of geomet rical complexity. Experiments results using new STSF, show the robot can avoid obstacles (boxes and trash can) and foll ow the wall. Figure 10 through Figure 11 demonstrate one o f many successful experiments. The algorithm is very effective in escaping local minima encountered in laboratory environments.

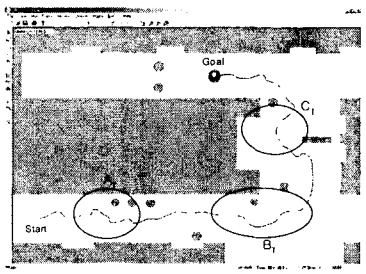

(a). Experiment in a corridor.

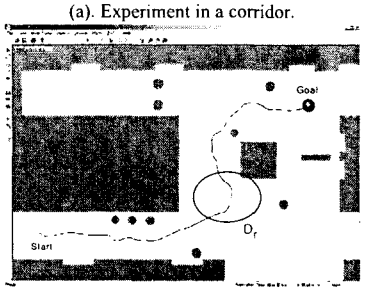

(b). Experiment in a corridor with wide space.

Fig. 11. Simulation used a STSF scheme.

The mobile robot navigates along a corridor with 3m width and with some obstacles as shown in Figure 10 and Figure 11. It demonstrates that the mobile robot avoids the obstacles intelligently and follows the corridor to the goal.

Also notice that especially at the region, A_T, the errors of the robot position converse to zero as the same reason, referring to the simulation result and experimental result in Figure. 10-(a) and 10-(b) respectively, Figure 11-(a) and 11-(b) represent the reference of robot direction produced by the proposed STSF. Finally, the robot is tested to follow the whole trajectory from start position to final position as shown in Figure 10 and Figure 11.

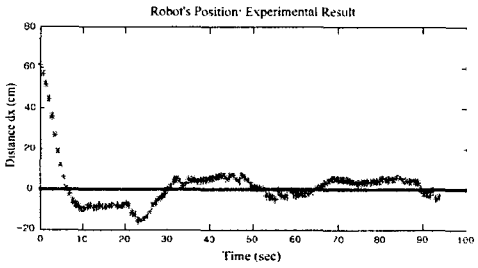

Fig. 12. Robot's position experiment results.

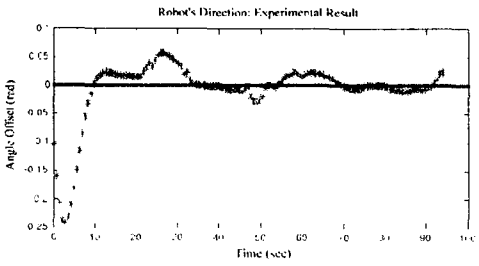

Fig. 13. Robot's direction experiment results.

The experimental results of the robot status for distance between mobile robot and corridor wall under such control strategy are given in Figure 12 and 13.

5.3. Experimental Comparison

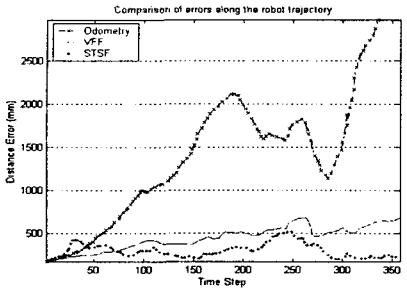

(a) distance error

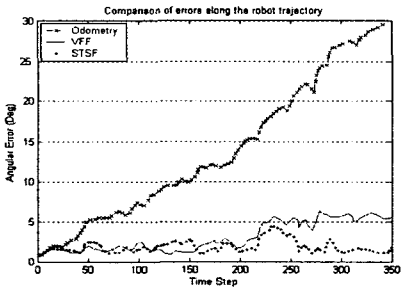

(b) angular error.

Fig. 14. Comparison of errors along the robot trajectory.

Table 4. Summary of the solution obtained by the different approaches.

Maximum errors (x_{max}, y_{max}, and ϕ_{max}), Distance d_{rel} and Angular ϕ_{rel} Error growing-rates, and $\aleph^2_{test}$ results.

	Odometry	VFF	STSF
x_{max}(mm)	1622.22	426.44	288.02
y_{max}(mm)	2144.70	355.62	202.65
ϕ_{max}(deg)	27.20	4.44	3.93
d_{rel}(mm/m)	47.4	10.8	7.8
ϕ_{rel}(deg/m)	0.432	0.144	0.114
$\aleph^2_{test}$(%)	100	6.7	97.2

Table 4 compares the largest errors obtained by the STSF method with the approach neglecting correlations. Clearly, the STSF method obtained estimations for the mobile robot localization with an upper bound of around 5.9 mm/m of the total trajectory length for the distance error and 0.04°/m for the orientation error, which represented an order of magnitude below dead-reckoning errors. Also, the location uncertainty of the map features was not underestimated, with a compatibility of $\aleph^2_{test} \cong 97\%$.

Therefore, pairings between local observations at time k and previously stored knowledge up to time k-1 were found at each point along the robot trajectory even when the vehicle returned to previously learned places of the navigation area. An average of 74% of the number of available observations were matched with previous known features. Figure 27 compares the real errors along the robot path, obtained by each approach. The highest errors correspond to odometry-based navigation, while the smallest correspond to the STSF method. From the Figure 27 note how the location uncertainty of the robot decreases when the vehicle revisits previously learned places (i.e., from trajectory point 40 onwards).

VI. Conclusions

In this paper, a new sensor fusion concept, STSF(space and time sensor fusion), was introduced. The effectiveness of STSF was demonstrated through the examples, simulations and experiments. To generate complete navigation trajectories without *a prior* information on the environment, not only the data from the sensors located at different places but also the previous sensor data are inevitably utilized. Although we have tried using the sonar system for map building and navigation in indoor environment, the result from the above experiments clearly shows that by utilizing both systems and applying active sensing to adapt to differing situation, a high level of competent collision avoidance behavior by STSF can be achieved.

Sonar system and visual systems are cooperatively utilized for collision avoidance based upon STSF such that a mobile robot was successfully navigated in an unstructured environment as well as in a structured environment. Based on these results, further experiments will aim at applying the proposed tracking technique to the multi-sensor fusion scheme which is applied to the control of a mobile robot in an unstructured environment.

Acknowledgements

The author would like to acknowledge financial support from Center for Intelligent & Integrated Port Management Systems[CIIPMS] at Dong-A university.

References

[1] R. C. Ruo and K. L. Su, "A Review of High-level Multisensor Fusion: Approaches and applications," *Proc. Of IEEE Int'l. Conf. On Multisensor Fusion and Integration for Intelligent Systems*, pp. 25-31, Taipei, Taiwan, 1999.

[2] J. M. Lee, B. H. Kim, M. H. Lee, M. C. Lee, J. W. Choi, and S. H. Han, "Fine Active Calibration of Camera Position/ Orientation through Pattern Recognition," *Proc. of IEEE Int'l. Symp. on Industrial Electronics*, pp. 100-105, Slovenia, 1999.

[3] M.e Kam, X. Zhu, and P. Kalata, "Sensor Fusion for Mobile Robot Navigation," *Proc. of the IEEE*, Vol. 85, No. 1, pp. 108-119, Jan. 1997.

[4] P. Weckesser and R. Dillman, "Navigating a Mobile Service-Robot in a Natural Environment Using Sensor-Fusion Techniques," *Proc. of IROS*, pp.1423-1428, 1997.

[5] J. Llinas and E. Waltz, "*Multisensor Data Fusion,*" Boston, MA:Artech House, 1990.

[6] D. Hall, "*Mathematical Techniques in Multisensor Data Fusion,*" Boston, MA: Artech House, 1992.

[7] L. A. Klein, "*Sensor and Data Fusion Concepts and Applications*," SPIE Opt, Engineering Press, Tutorial Texts, vol 14, 1993.

[8] H. R. Beom and H. S. Cho, "A sensor-Based Navigation for a Mobile Robot Using Fuzzy Logic and Reinforcement Learning," *IEEE Trans. on system, man, and cybernetics*, Vol.25, No. 3, pp.464-477, March 1995.

[9] A. Ohya, A. Kosaka and A. Kak, "Vision-Based Navigation by a Mobile Robot with Obstacle Avoidance Using Single-Camera Vision and Ultrasonic Sensing," *IEEE Transactions on Robotics and Automation*, Vol. 14, No. 6, pp. 969-978, December 1998.